Separation Science and Technology
Publication details, including instructions for authors and subscription information:
http://www.informaworld.com/smpp/title~content=t713708471

Lithium Type X Zeolite as a Superior Sorbent for Air Separation

M. S. A. Baksh[a]; E. S. Kikkinides[a]; R. T. Yang[a]
[a] DEPARTMENT OF CHEMICAL ENGINEERING, STATE UNIVERSITY OF NEW YORK AT BUFFALO, BUFFALO, NEW YORK

To cite this Article Baksh, M. S. A. , Kikkinides, E. S. and Yang, R. T.(1992) 'Lithium Type X Zeolite as a Superior Sorbent for Air Separation', Separation Science and Technology, 27: 3, 277 — 294
To link to this Article: DOI: 10.1080/01496399208018880
URL: http://dx.doi.org/10.1080/01496399208018880

SEPARATION SCIENCE AND TECHNOLOGY, 27(3), pp. 277–294, 1992

Lithium Type X Zeolite as a Superior Sorbent for Air Separation

M. S. A. BAKSH, E. S. KIKKINIDES, and R. T. YANG*
DEPARTMENT OF CHEMICAL ENGINEERING
STATE UNIVERSITY OF NEW YORK AT BUFFALO
BUFFALO, NEW YORK 14260

Abstract

Li-X, Ba-X, and Li-A zeolites are prepared by ion exchange with the commercial Na-X (13X) and Na-A (4A) zeolites. At the ambient temperature (298 K), only Li-X exhibits a significant enhancement of the N_2/O_2 adsorption selectivity over the commercial zeolites. At a pressure of 1 atm, the N_2/O_2 selectivity is increased from approximately 3 for 13X and 4A to approximately 7 for Li-X. Air separations by the two sorbents Li-X and Na-X are compared using a commercial 5-step air-separation pressure swing adsorption (PSA) cycle. The comparison is made by using a mathematical model of proven predictive ability. A parametric comparison shows superior separation results for the Li-X zeolite under all PSA conditions. For example, the Li-X sorbent gives >90% O_2 purity and an O_2 recovery of over 70% at a feed rate of $>5.65 \times 10^5$ L STP/h. In addition, for the same O_2 purity and feed rate, the Na-X sorbent gives an O_2 recovery of less than 30%. Hence the replacement of the commercially used Na-X sorbent by the Li-X sorbent will result in an energy saving of over 50%.

INTRODUCTION

Pressure swing adsorption (PSA) has received substantial attention due to its vast potential in the separation of mixtures, and has been commercialized for air separation, hydrogen purification, air drying, and other separations (*1*). Inherent to adsorption processes is the use of an adsorbent to bring about separation by one or more of the following mechanisms: steric, kinetic, and/or equilibrium. In the case of the steric effect, only small, well-shaped molecules can diffuse into the adsorbent. Kinetic separation is achieved by virtue of the differences in diffusion rates of the various molecules into the adsorbent, and the equilibrium effect operates through the competitive adsorption of the adsorbates.

*To whom correspondence should be addressed.

The separation of air is of proven commercial importance. For instance, oxygen can be used in the manufacture of steel, welding of materials, and therapeutic utilization, whereas nitrogen can be used in enhanced oil recovery and in N_2-based controlled atmospheres in the food and metallurgical industries. Currently, the large-scale separation of air is effected by the costly cryogenic process in which the air is cooled to temperatures near the boiling points of -183 and -196°C for O_2 and N_2 respectively, at atmospheric pressure. However, for small-to-medium-scale production of O_2 and N_2, PSA is more economical. Presently, 5A and Na-X are being used for the equilibrium separation of air (*1–6*), whereas 4A zeolite and carbon molecular sieves (*7*) have been used for the kinetic separation of air by PSA (*8, 9*). However, the low equilibrium selectives (N_2/O_2) of about 2–3 on 5A and Na-X zeolites, and the relatively small kinetic selectivity on 4A and CMS of about 30 limit the efficiency of the systems. For example, in the PSA process developed by Bergbau-Forschung GmbH using CMS (*7*), the N_2 product contains 95–99% (N_2 + Ar), and the N_2 recovery was $\leq$50% (*9*). In addition, PSA processes using 5A zeolite produced only 85–95% O_2 purity at 10–30% O_2 recovery (*10*).

The chemical composition of the zeolite molecular sieves (e.g., 5A and Na-X) can be varied by ion exchange of its cations, which in turn alters the pore dimensions and adsorption potentials to bring about different equilibrium/kinetic selectivities. For these adsorbents (5A and Na-X zeolites), the preferential adsorption of N_2 from air is due to the greater molecular interactions between the quadrupole moment of N_2 and the zeolites. From a practical standpoint, the higher equilibrium selectivities of N_2/O_2 imply the use of a smaller size adsorbent bed to produce a given quantity of O_2 at the desired purity. With the X-type zeolite ion exchanged for alkali and alkaline earth metal cations, McKee (*11*) observed enhanced N_2/O_2 selectivities at -78°C, most prominently for Li-X and Ba-X. However, it was not known whether the enhanced selectivities would hold at the ambient temperature, and whether the ion-exchanged A-type zeolite would also have enhanced selectivities. These important questions are answered in this work.

In this study, Na-X zeolite was ion exchanged to produce Li-X and Ba-X zeolites according to the procedures outlined by McKee (*11*) and Sherry (*12*). Li-A was also prepared from Na-A zeolite (the 4A zeolite). The adsorption isotherms of N_2 and O_2 were measured using a volumetric system for pressures above 1.0 atm and a thermogravimetric analyzer for subatmospheric pressures. The isotherm results were then used in a nonisothermal equilibrium PSA model to obtain theoretical results of a PSA process using Li-X and Na-X zeolites. The simulation results show that Li-X always gives better O_2 purity and O_2 recovery when compared to Na-X. Oxygen

purity ≥90% and O_2 recovery ≥70% were obtained for air separation at a feed rate of ≥5.65 × 10^5 L STP/h.

EXPERIMENTAL

Preparation of Ion-Exchanged X and A Zeolites

The starting material for the X zeolite was Linde Na-X (13X) 8 × 12 mesh beads (Lot No. 945186030170). The lithium chloride and barium chloride were purified grade from Fisher Scientific. The experimental procedure for Li-X is described below.

The first step in the ion exchange is the preparation of 0.1 *M* LiCl solution. This was accomplished by dissolving the equivalent amount of the salt in deionized distilled water at room temperature. The next step was ion exchanging of Li^+ cations with the Na^+ cations. This was done by percolating a hot 0.1 *M* LiCl solution through a bed of Na-X zeolite. A schematic of the ion-exchange apparatus is shown in Fig. 1. The total volume of LiCl solution used was 4.0 L, which percolated through a zeolite bed containing 7.0 g of Na-X zeolite at an effluent flow rate of 1.8 cm^3/min. The ion-exchange reaction took about 36 h and was conducted at 85°C. The water bath temperature was kept uniform with the aid of a magnetic stirrer, and any loss of water due to evaporation was replaced with water at 85°C in order to suppress any temperature gradients. The adsorbent was then transferred to a filtering manifold and washed several times with deionized distilled water to remove the LiCl. Washing was terminated when no precipitation was observed upon the addition of $AgNO_3$ to filtrate. The Li-X zeolite was calcined at 400°C for 10 h before being stored in a capped polyethylene bottle. A similar procedure was used to prepare Ba-X zeolite.

Li-A type zeolite was also prepared by ion exchange of the Na-A zeolite (4A zeolite) with the Li^+ cations.

Isotherm Measurements

Equilibrium isotherms for subatmospheric pressures were measured using a microbalance (Mettler TA2000C Thermoanalyzer) which was connected to a gas flow system, while a static volumetric system was used for pressures above 1.0 atm. The gases were purchased from Cryogenic Supply (Union Carbide, Linde Division), and the purity specifications were nitrogen (99.99%), helium (99.995%), and oxygen (99.995%). Each of the gases was passed through a molecular sieve (Linde 5A) bed to remove traces of water and other impurities. The molecular sieve was regenerated period-

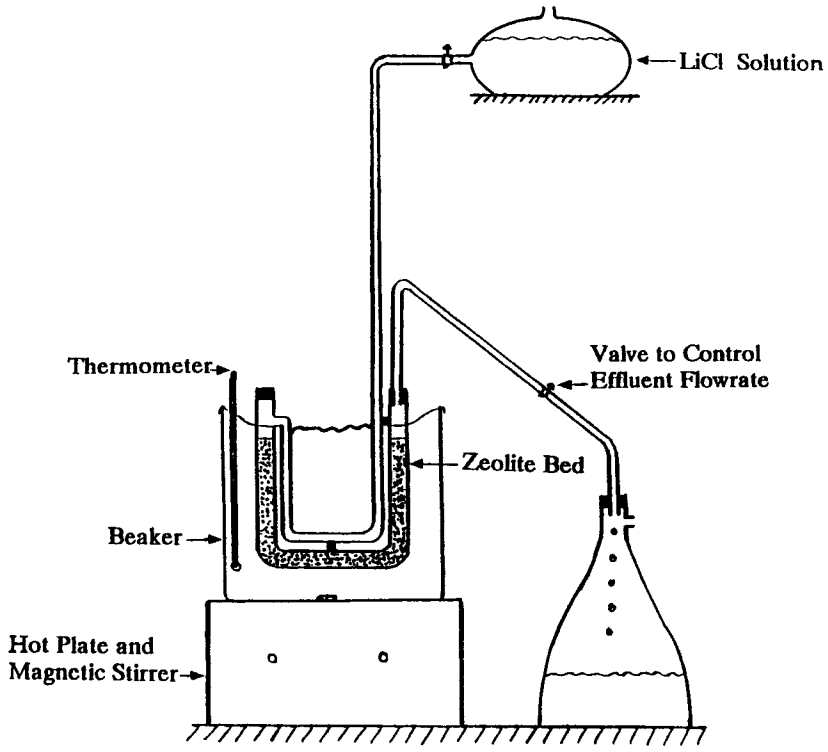

FIG. 1. Schematic of the ion-exchange apparatus.

ically by heating at 350°C for about 20 h under vacuum. Prior to isotherm determination, each sample was outgassed *in situ* at 350°C for 15 h.

In addition to the experimental data obtained from this work, additional N_2 and O_2 sorption data on Na-X (13X) were taken from the literature (*13*) and used for comparison with our results, and in some cases, to supply input data to our PSA model.

PSA AIR SEPARATION

PSA Cycle

A variety of PSA cycles have been reviewed by Yang (*1*), Tondeur and Wankat (*14*), and Sircar (*15*). The fundamental steps in any PSA cycle consist of pressurization, adsorption, and depressurization. The feed mixture or light component product from another bed can be used in the

pressurization step, whereas cocurrent blowdown followed by countercurrent depressurization (*16, 17*) or cocurrent heavy component purge followed by countercurrent depressurization (*18–20*) can be used for the depressurization step.

The PSA cycle used in this work is essentially the same as that used in industry for air separation, and consists of the following steps:

Step I: Light component (O_2) pressurization
Step II: High pressure adsorption
Step III: Cocurrent depressurization
Step IV: Countercurrent blowdown
Step V: Countercurrent purge with product (at low pressure)

Typically, three or more beds are operated together, so that continuous feed and product are possible.

The PSA process performance is judged by the following factors: product purity, product recovery, and feed throughput, all at cyclic steady state. The effluents from Steps II and III are collected at O_2 product, whereas the effluents from Steps IV and V are collected as N_2 product. The O_2 product purity is then defined as the volume-averaged concentration over the effluent from Steps II and III, and N_2 product purity is the volume-averaged concentration over the effluent from Steps IV and V. The product purities are expressed as mol%. The product recoveries are defined as follows:

$$O_2 \text{ recovery} = \frac{(O_2 \text{ from Steps II and III}) - (O_2 \text{ used in Steps V and I})}{(O_2 \text{ in the feed used in Step II})}$$

$$N_2 \text{ recovery} = \frac{N_2 \text{ from Steps IV and V}}{N_2 \text{ in the feed used in Step II}}$$

Mathmematical Model

An adiabatic model has been developed to simulate an adsorber bed going through various PSA cycle steps. The model is based on the following assumptions: The mass transfer resistance is negligible, there is no radial dependence of both concentration and temperature, the flow pattern is described by the plug flow model, the axial pressure drop is negligible, and the ideal gas law applies.

The total mass balance in the bed can be written as

$$\epsilon \frac{\partial C}{\partial t} + \frac{\partial uC}{\partial z} + \rho_B \frac{\partial q}{\partial t} = 0 \tag{1}$$

Similarly, the mass balance equations for each of the species are

$$\epsilon \frac{\partial C_i}{\partial t} + \frac{\partial u C_i}{\partial z} + \rho_B \frac{\partial q_i}{\partial t} = 0, \qquad i = 1, 2, \ldots, N \tag{2}$$

where $C_i = Py_i/RT$ and $q = \Sigma q_i$

The heat balance equation assuming adiabatic conditions becomes

$$(\epsilon C c_{pg} + \rho_B c_{ps}) \frac{\partial T}{\partial t} + C c_{pg} u \frac{\partial T}{\partial z} + \rho_B \sum H_i \frac{\partial q_i}{\partial t} = 0 \tag{3}$$

where $c_{pg} = \Sigma c_{pi} y_i$

If the resistance to mass transfer is negligible (equilibrium model), we have

$$\frac{\partial q_i}{\partial t} = \frac{\partial q_i^*}{\partial t} \tag{4}$$

where q_i^* is the equilibrium amount adsorbed.

The equilibrium mixture adsorption can be calculated by the extended Langmuir isotherm:

$$q_i^* = \frac{K_i P_i}{1 + \sum B_j P_j}, \qquad i = 1, 2, \ldots, N \tag{5}$$

where

$$K = k_1 e^{k2/T} \qquad \text{and} \qquad B = k_3 e^{k4/T}$$

The values of k_1, k_2, k_3, and k_4 are given in Table 1.

Initial and Boundary Conditions

The adsorption column was assumed to contain initially pure O_2. Thus,

At $t = 0$ and $0 < z < L$, $y_i = x_i = 1$ for $i = O_2$
At $t = 0$ and $0 < z < L$, $y_i = x_i = 0$ for $i = N_2$
At $t = 0$ and $0 < z < L$, $P = P_H$

where $x_i = q_i/q$.

TABLE 1
Values for the Constants in the Temperature-Dependent Langmuir Equation (see Eq. 5)

Sorbent	Sorbate	k_1, mmol/g·atm	k_2, K^{-1}	k_3, atm^{-1}	k_4, K^{-1}	$-H$, cal/mol	c_p, cal/mol·K
Na-X	O_2	1.07×10^{-3}	1592.53	8.31×10^{-5}	1544.43	3160	8.27
Na-X	N_2	2.9×10^{-4}	2168.55	1.17×10^{-4}	2012.92	4310	6.50
Li-X	O_2	3.24×10^{-4}	1592.53	3.29×10^{-5}	1544.43	3160	8.27
Li-X	N_2	4.22×10^{-4}	2168.55	2.42×10^{-4}	2012.92	4310	6.50

The boundary conditions for the ensuing cycles are:

STEP II. High-pressure adsorption:

At $z = 0$, $y_i = y_{f,i}$
At $z = 0$, $T = T_0$
At $z = 0$, $u = u_f$
$P = P_H$

STEP III. Cocurrent depressurization:

At $z = 0$, $\partial y_i/\partial z = 0$
At $z = 0$, $\partial T/\partial z = 0$
At $z = 0$, $u = 0$
$P = P(t)$

STEP IV. Countercurrent blowdown:

At $z = L$, $\partial y_i/\partial z = 0$
At $z = L$, $\partial T/\partial z = 0$
At $z = 0$, $u = u_f$
$P = P_H$

STEP V. Countercurrent purge:

At $z = L$, $y_i = y_{p,i}(t)$
At $z = L$, $T = T_0$
At $z = L$, $u = u_{purge}$
$P = P_L$

where $y_{p,i}(t)$ is the instantaneous effluent mole fraction of species i during Step II.

STEP I. Light component pressurization:

At $z = 0$, $y_i = y_{p,i}(t)$
At $z = L$, $T = T_0$

At $z = L$, $u = 0$
$P = P(t)$

The initial conditions for each step are the conditions at the end of the preceding step. Note that the pressure history is an input in PSA and is represented usually by a quadratic form:

$$P(t) = a_0 + a_1 t + a_2 t^2 \tag{6}$$

In the present study $a_2 = 0$, resulting in a linear dependence of pressure with time.

The adsorber characteristics together with the operating conditions for the standard case are listed in Table 2. A 20-min cycle was used in the simulations with the following distribution:

Step I: 4.0 min
Step II: 4.0 min
Step III: 4.0 min
Step IV: 4.0 min
Step V: 4.0 min

This model has been used successfully in predicting experimental PSA results (*16*, *19*).

Numerical Solution of the Model

The implicit backward finite difference scheme used previously in this laboratory for PSA model simulations was employed in the present work

TABLE 2
Adsorption Bed Characteristics and Operating Conditions for the Standard Simulation

Adsorber bed	Operating conditions
	Feed composition, %:
Bed length: 500 cm	$N_2/O_2/Ar$ = 78/21/1
Bed diameter: 100 cm	Feed rate: 6.85×10^5 L STP/h
Void fraction (ϵ): 0.75	P/F = 0.08
	P_H = 5 atm
	P_{III} = 2.5 atm
Bed density: 0.72 g/cm^3	P_L = 1 atm
	Total cycle time: 20 min
	Ambient temperature, T_0 = 298 K

to solve Eqs. (1), (2), and (3) combined with (4) and (5). Furthermore, the modifications in the numerical technique described by Kikkinides and Yang (*21*) were also employed in the present work in order to achieve faster convergence. In a typical computation, 80 space and 2500 time steps were used for each PSA cycle. The model was always stable and convergent at least in the range of conditions used in this study. All computations were performed using a VAX-780 computer. It took approximately 3 min of CPU time for each cycle and it generally took beween 20 and 30 cycles to reach cyclic steady state.

RESULTS AND DISCUSSION

Adsorption Isotherms

The replacement of the Na^+ cation in Na-X (13X) zeolite by ion exchange with other cations produced zeolites having different pore sizes, chemical composition, and different physical properties (*22*). In particular, McKee (*11*) found that cations such as Sr^{2+}, Li^+, Ba^{2+}, and Ni^{2+} present in zeolites give a marked increase in the N_2/O_2 equilibrium selectivity at $-78°C$. Although this phenomenon is not completely understood, it is generally agreed that the preferential adsorption of N_2 over O_2 is due to the strong interaction between the quadrupole moment of the N_2 molecule and the zeolite.

In this study, only Li-X showed significantly enhanced selectivities at the ambient temperature. The enhanced N_2 adsorption on Li-X zeolite is displayed in Figs. 2 and 3. The results of Fig. 2 correspond to the low pressure adsorption isotherms using a thermogravimetric analyzer whereas the Fig. 3 results were obtained from a high pressure static volumetric system. The selectivity ratio, expressed as the amount adsorbed N_2/amount adsorbed O_2 at the same pressure is shown as a function of pressure in Fig. 4 for Li-X and Na-X zeolites. It is obvious from Fig. 4 that the selectivity (N_2/O_2) ratio on Li-X is about twice that of Na-X for pressures below 5.0 atm.

Significantly, no enhanced N_2/O_2 selectivities were observed at 298 K for Ba-X and Li-A zeolites over their Na-form counterparts. This result is in direct contrast to McKee's observation of the high enhancement for the Ba-X zeolite at $-78°C$ (*11*).

In the following three sections, all of the PSA theoretical results were obtained from air having 78 mol% N_2, 21 mol% O_2, and 1 mol% Ar. The isotherms of argon on zeolite type X are almost identical to the oxygen isotherms (*1*). Thus, in the PSA simulation, argon was collected as raffinate along with oxygen, and the O_2 purity was calculated by multiplying the

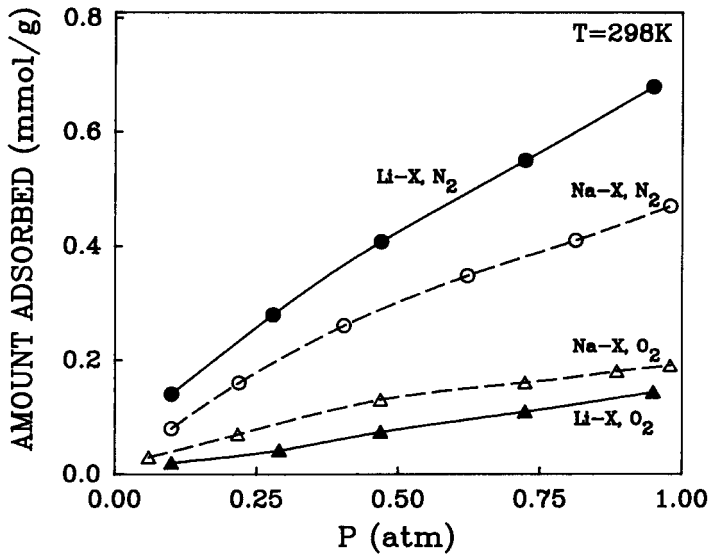

FIG. 2. Low pressure adsorption isotherms of O_2 and N_2 at 298 K.

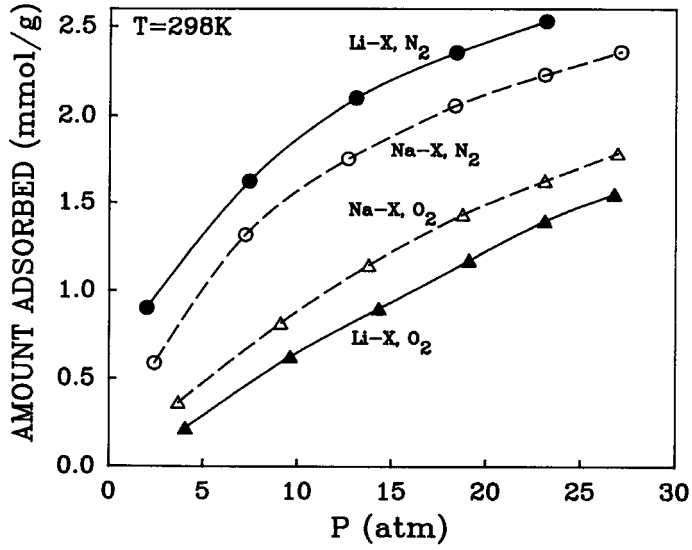

FIG. 3. High pressure adsorption isotherms of O_2 and N_2 at 298 K.

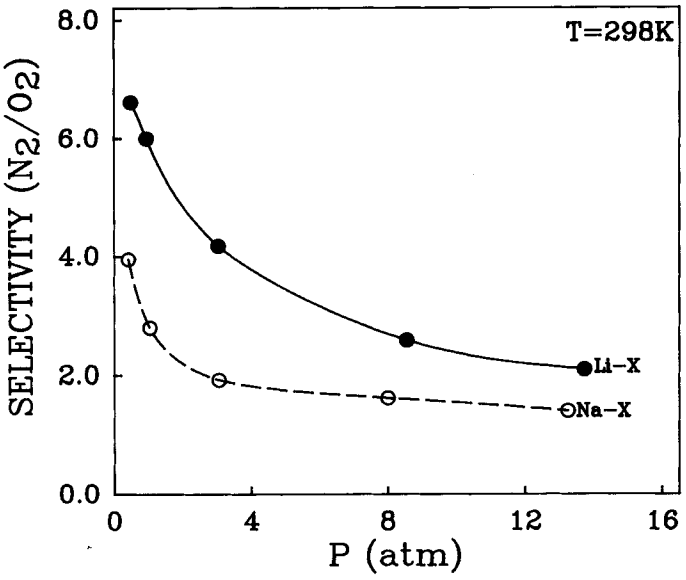

FIG. 4. Adsorption selectivity ratio for N_2/O_2 at 298 K.

raffinate by the ratio 21/22. Therefore, the limiting purity for O_2 is approximately 95.5 mol%.

Effect of P/F Ratio on the Product Purity and Recovery

The purge gas employed in the five-step cycle was obtained from a portion of the Step II product. The purge/feed ratio (P/F) is defined as:

$$\frac{P}{F} = \frac{\text{purge gas used in Step V}}{\text{total } O_2 \text{ in feed}}$$

The effect of P/F ratio on PSA separation has been studied extensively (*1*). The results of Fig. 5 show that an increase in the P/F ratio gives higher light product purity for values of P/F below a certain threshold value. Beyond this threshold value, any further increase in P/F has no effect on the product purity. Thus, by increasing P/F up to a certain value, a cleaner bed was produced at the end of Step V, which allows for a sharper O_2 wavefront in Step II, resulting in a higher O_2 purity. However, higher P/F has the disadvantage of lowering the product recovery due to the loss of more O_2 in the N_2 effluent. In addition, it is evident from Fig. 5 that as

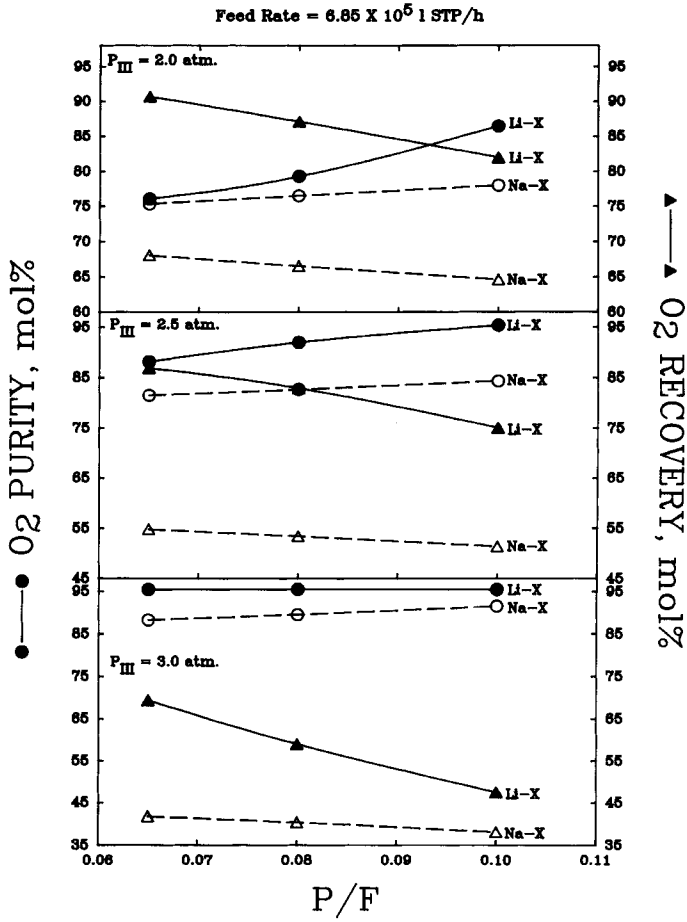

FIG. 5. Effect of P/F on the O_2 purity and recovery.

the end pressure of cocurrent depressurization (P_{III}) is decreased, a higher P/F is needed to produce O_2 with the same purity.

The purity of the heavy product (N_2) increases with decreasing P/F, and levels off below a certain value of P/F. On the other hand, the recovery of N_2 declines as P/F decreases. The results of Fig. 6 indicate that N_2 purity levels off at P/F = 0.1 for Na-X but not for Li-X. In addition, it should be noted that the dominant factor that limits the heavy component purity is the gas remaining in the void space prior to the desorption step.

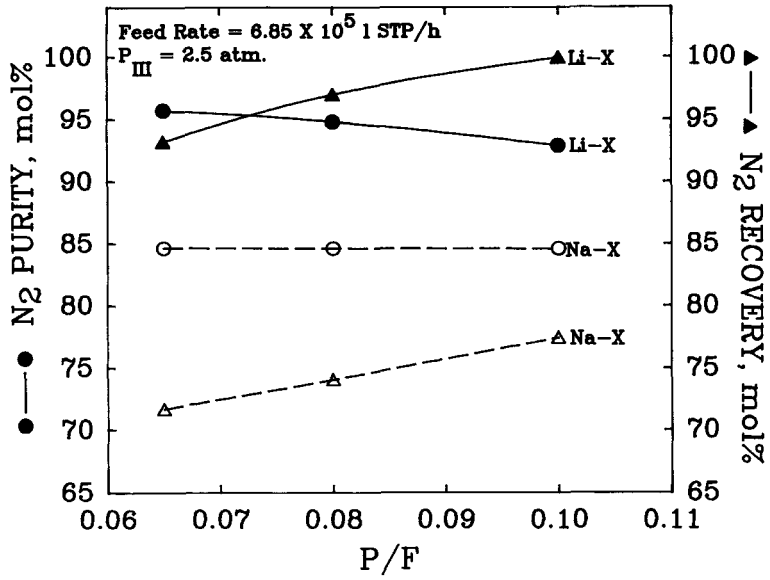

FIG. 6. Effect of P/F ratio on the N_2 purity and recovery.

Effect of End Pressure of Cocurrent Depressurization

The effect of end pressure of cocurrent depressurization (P_{III}) at three different feed rates (5.65×10^5, 6.85×10^5, and 8.06×10^5 L STEP/h) and at P/F = 0.08 are displayed in Fig. 7. Larger values of P_{III} increase O_2 purity and decrease O_2 recovery. Since the adsorption isotherms of N_2 and O_2 on Li-X and Na-X are favorable, the wavefronts of these components (N_2 and O_2) broaden as the pressure is lowered (*1*). Consequently, as P_{III} decreases, the N_2 wavefront becomes more diffused, resulting in higher contamination of the O_2 product (lower purity). The higher O_2 recovery at lower P_{III} simply indicates that more O_2 was recovered from the bed voids during the cocurrent depressurization step. The results of Fig. 7 also indicate that as the feed rate increases, a higher P_{III} is needed to obtain the same O_2 purity. The results of Fig. 8 show when P_{III} decreases, the N_2 purity increases, and its recovery decreases.

Effect of Feed Rate on the Product Purity and Recovery

The effect of air feed rate was studied by varying the feed rate from 5.65×10^5 to 8.06×10^5 L STP/h for the same amount of sorbent, while the other process variables were kept constant. The results for three values of P/F (0.065, 0.08, and 0.1) at a constant end pressure of cocurrent

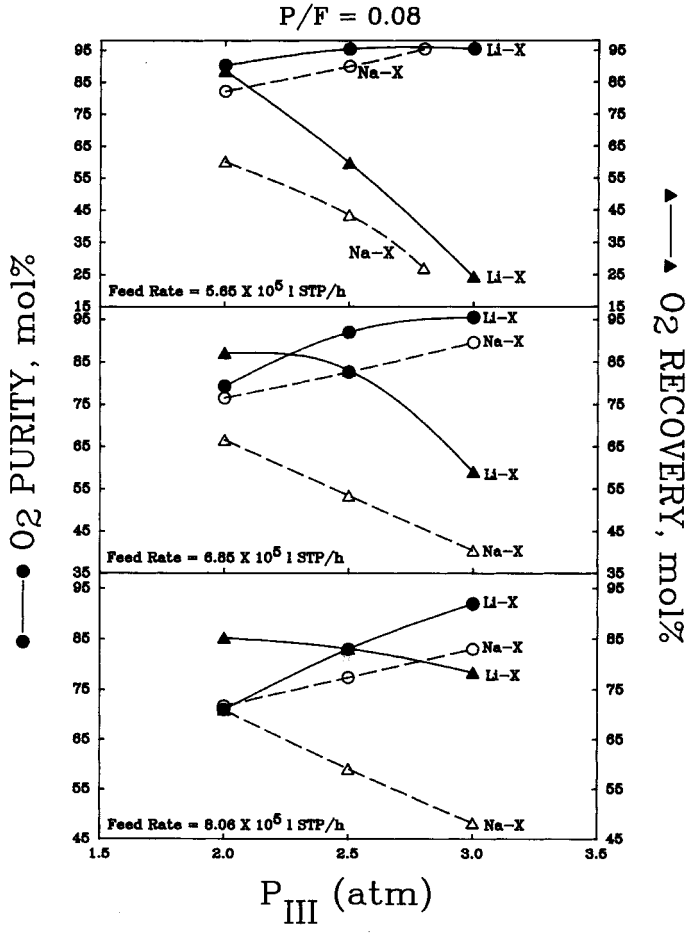

FIG. 7. Effect of end pressure of cocurrent depressurization (P_{III}) on the O_2 purity and recovery.

depressurization (P_{III} = 2.5 atm) are displayed in Fig. 9. It is obvious from the figure that higher feed rate gives lower O_2 purity and improves the O_2 recovery. Such results can be explained in terms of the bed utilization, which is defined as the fraction of the bed covered by the heavy component (N_2) during Step II of the PSA cycle. The higher feed rate increases the bed utilization and produces an early breakthrough (in Step III) of N_2,

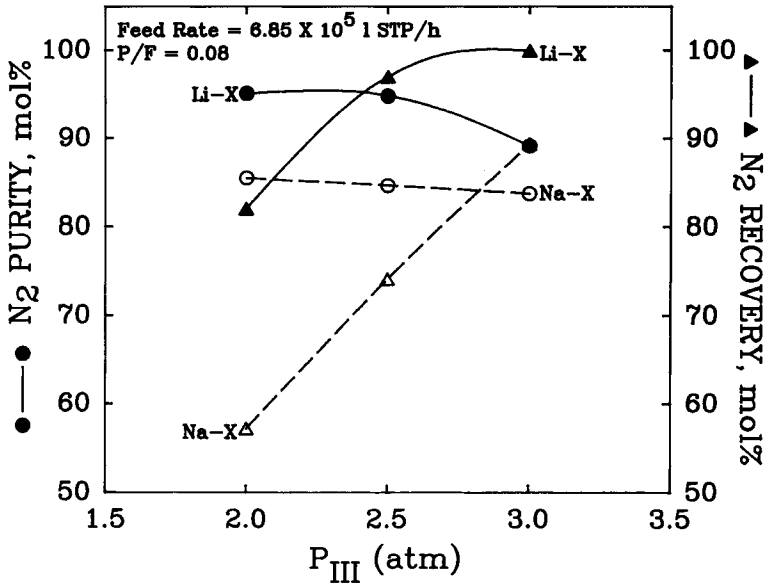

FIG. 8. Effect of end pressure of cocurrent depressurization (P_{III}) on the N_2 purity and recovery.

which lowers the O_2 purity and enhances the O_2 recovery from the voids (in Step III). In addition, the results of Fig. 9 also indicate that as P/F increases, a higher feed rate can be accomplished for the same O_2 purity. The results of Fig. 10 show that higher feed rate increases N_2 purity, while N_2 recovery decreases.

NOMENCLATURE

B	Langmuir constant (atm^{-1}), in Eq. (5)
C	concentration in bulk flow (mol/cm^3)
c_p	heat capacity (cal/mol·K)
H	heat of adsorption (cal/mol)
K	Langmuir constant (mol/g·atm), in Eq. (5)
L	length of the bed (cm)
N	total number of components in the mixture
P	pressure (atm)
q	moles adsorbed per gram of solid (mol/g)
R	gas constant

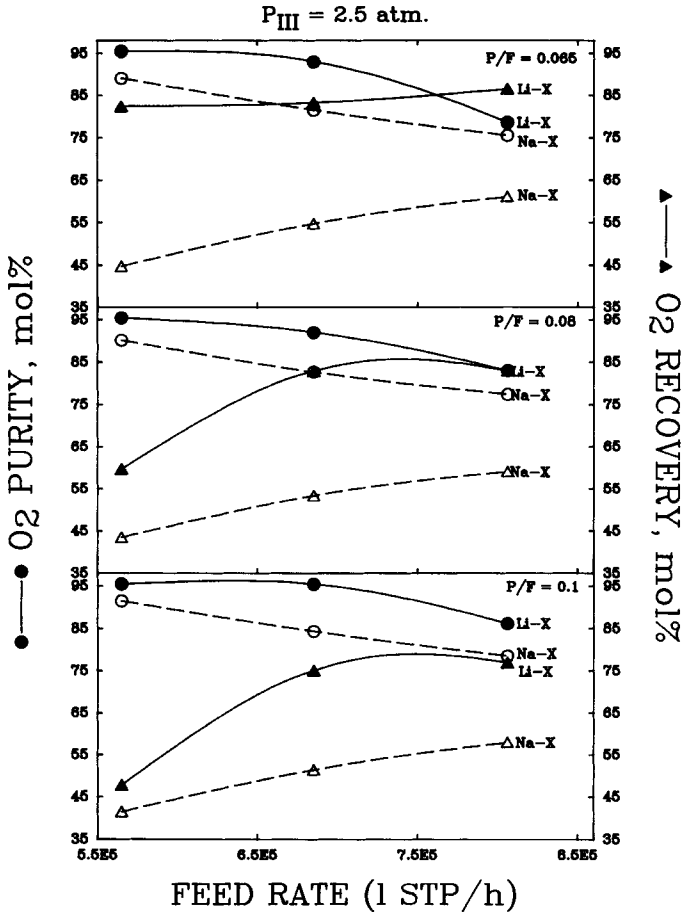

FIG. 9. Effect of feed rate on the O_2 purity and recovery.

T	temperature in the bed (K)
T_0	ambient temperature (K)
t	time (s)
u	superficial velocity (cm/s)
x	mole fraction in the adsorbed phase
y	mole fraction in the gas phase
z	axial position in the bed (cm)

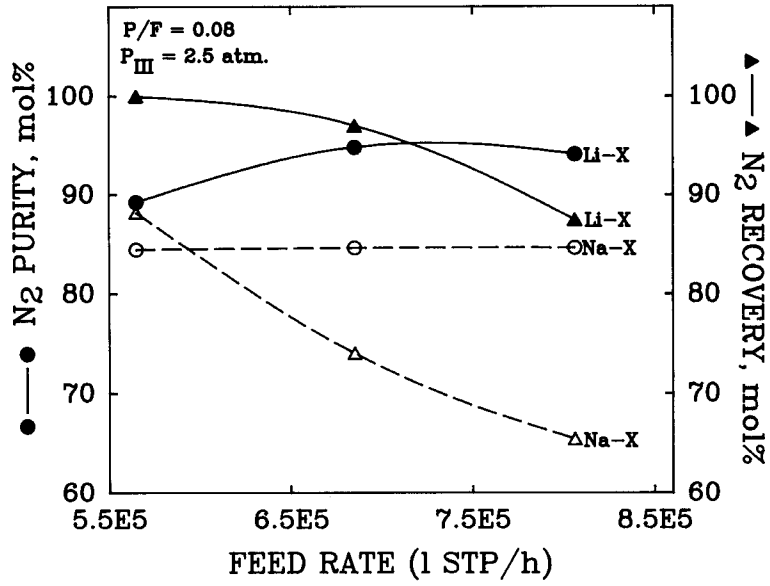

FIG. 10. Effect of feed rate on the N_2 purity and recovery.

Greek Letters

ϵ	fractional void in the bed
ρ_B	density of the bed (g/cm^3)

Subscripts

B	bed
f	feed
g	gas phase
H	high
i	Species i
j	Species j
L	low
p	product
s	solid phase

Superscript

*	equilibrium

Acknowledgment

This work was supported by the NSF under Grant CTS-8914754.

REFERENCES

1. R. T. Yang, *Gas Separation by Adsorption Processes,* Butterworths, Boston, 1987.
2. S. Sircar, "Preparation of High Purity Oxygen," U.S. Patent 4,756,723 (1988).
3. S. Sircar and J. W. Zondlo, "Fractionation of Air by Adsorption," U.S. Patent 4,013,429 (1977).
4. S. Sircar, R. R. Conrad, and W. J. Ambs, "Binary Ion Exchanged Type X Zeolite Adsorbent," U.S. Patent 4,557,736 (1985).
5. J. J. Collins, "Air Separation by Adsorption," U.S. Patents 3,973,931 (1976) and 4,026,680 (1977).
6. C. W. Kratz and S. Sircar, "Production of Oxygen Enriched Air," U.S. Patent 4,685,939 (1987).
7. H. Juntgen, *Carbon, 15,* 273 (1977).
8. Z. J. Pan, R. T. Yang, and J. A. Ritter, "Kinetic Separation of Air by Pressure Swing Adsorption," in *New Directions in Sorption Technology* (G. E. Keller II and R. T. Yang, eds.) Butterworths, Boston, 1989.
9. K. Knoblauch, *Chem. Eng., 87* (November 6, 1978).
10. R. T. Cassidy and E. S. Holmes, *AIChE Symp. Ser., 80*(233), 68 (1984).
11. D. W. McKee, "Separation of an Oxygen Nitrogen Mixture," U.S. Patents 3,140,932 and 3,140,933 (1964).
12. H. S. Sherry, *J. Phy. Chem., 70,* 1158 (1966).
13. G. W. Miller, *AIChE Symp. Ser.,* 259(83) (1987).
14. D. Tondeur and P. C. Wankat, *Sep. Purif. Methods, 14*(2), 157 (1985).
15. S. Sircar, in *Adsorption: Science and Technology* (A. E. Rodrigues, M. D. LeVan, and D. Tondeur, eds.), Kluwer, Boston, 1989, p. 285.
16. R. T. Yang and S. J. Doong, *AIChE J., 31,* 1829 (1985).
17. A. Kapoor and R. T. Yang, *Sep. Sci. Technol., 23*(1–3), 153 (1988).
18. M. S. A. Baksh, A. Kapoor, and R. T. Yang, *Ibid., 25*(7–8), 845–868 (1990).
19. P. L. Cen and R. T. Yang, *Ibid., 21*(9), 845 (1986).
20. S. Sircar, *Ibid., 23*(6–7), 519 (1988).
21. E. S. Kikkinides and R. T. Yang, *Ind. Eng. Chem., Res., 30,* 1981 (1991).
22. D. W. Breck, *Zeolite Molecular Sieves,* Wiley (Interscience), New York, 1974.

Received by editor March 12, 1991